# The Physics of a Climbing Rope

Dec. 2015

Ulrich Leuthäusser

In this theoretical paper the force-elongation behaviour of a climbing rope in a heavy fall is investigated and compared with experiments. At the beginning of the fall the rope has to be described by a nonlinear elastic force with negligible friction followed by a fast relaxation into equilibrium dominated by friction. Observed fast second mode oscillations are explained by a continuum description of the rope taking into account its mass.

## 1. Introduction

Modern climbing ropes have to fulfill many requirements. They must be light and flexible with high breaking strength and durability. They must be very elastic to reduce the peak forces of a heavy fall as well as highly energy absorbing so that the duration of the fall is as short as possible without back swings. This viscoelastic behaviour is investigated in this paper using measurements of the rope tension over time for standard UIAA falls. It is organized as follows.

After presenting the experimental facts in the next chapter, we provide in chapter 3 the necessary theoretical background. The so-called Standard Linear Solid (SLS) model in a mechanical formulation is introduced together with more general viscoelastic integral equations.
In chapter 4 the undamped harmonic oscillator (HO), the Maxwell model and the Kelvin model as special cases of the SLS are presented. From the HO the popular impact force formula follows, often used to describe the maximum tension of a climbing rope. However, the applicability of the HO model is limited because one also has to take into account friction as well as nonlinear forces.
Therefore in chapter 5 the friction mechanism of a climbing rope is discussed in detail. An important result is that friction is time-delayed beginning only near the force maximum to agree with the experiments. For an explanation, an excursion to thermodynamics is made. In chapter 6 it is shown that a linear model with time-delayed friction gives already a reasonable description of a climbing rope. For a more accurate description, however, an additional nonlinear component of the force, yielding the so-called Duffing oscillator, is necessary. One fall experiment where mass and fall height are varied independently can only be explained with that nonlinearity.
So far, the mass of the rope has been neglected. In chapter 7 a wave equation for the rope is derived which incorporates its mass in order to explain fast second mode oscillations which appear in the rope tension during the fall.

## 2. The experimental facts

In the standardized UIAA test fall[1], schematically shown in Fig.2.1, a climbing rope has to stop a 80kg mass m after its free fall of a distance h = 2 x 2.3m. The rope length is L = 2.6m so that the fall factor f = h/L is 1.77, near its maximum value 2.
In this heavy fall, the rope is strongly deformed and its tension F(t) is measured during the fall. We use very accurate measurements of[2] in time steps of 0.5 msec (Fig.2.2, red curve, Edelrid Cobra 10.3mm) where even small high frequency oscillations can be seen. They are important and are discussed in chapter 7.
The maximum tension $F_{max}$ of the above rope is 9.2kN and occurs after $t_1 \approx 160$ msec. $F_{max}$ is an important characteristic and has to be documented for every climbing rope by the rope manufacturer.

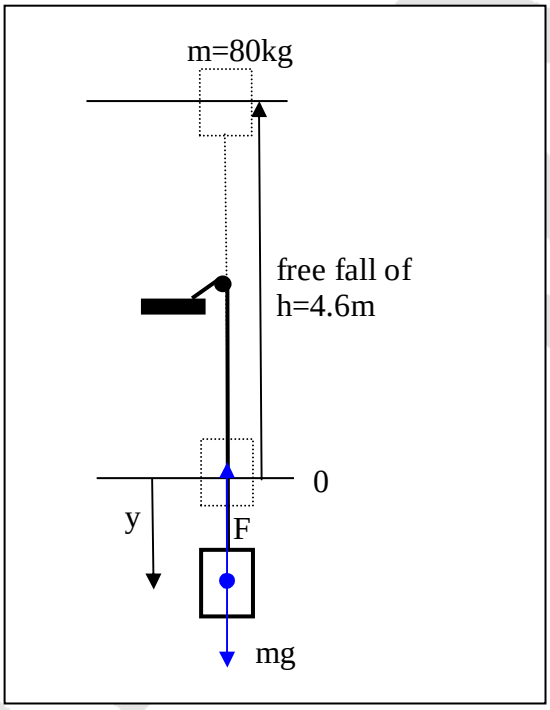


**Fig. 2.1.** Geometry of the test fall: after a free fall of 4.6m, a mass of 80kg starts to stretch the rope at 0. The rope tension is F and the elongation is y.

Although the tension F(t) can be very complicated with elastic and frictional parts, it is simply related to the acceleration $\ddot{y}(t)$ by Newton's equation of motion

$$m\ddot{y}(t) = mg - F(t) \qquad (2.1)$$

Two integrations of $\ddot{y}(t)$ with the initial conditions $v_0 = \sqrt{2gh}$ and $y_0 = 0$ lead to the velocity v(t) and the elongation y(t), both shown in Fig.2.2. The maximum elongation $y_{max}$ is 1.14m and has also to be reported for every climbing rope.

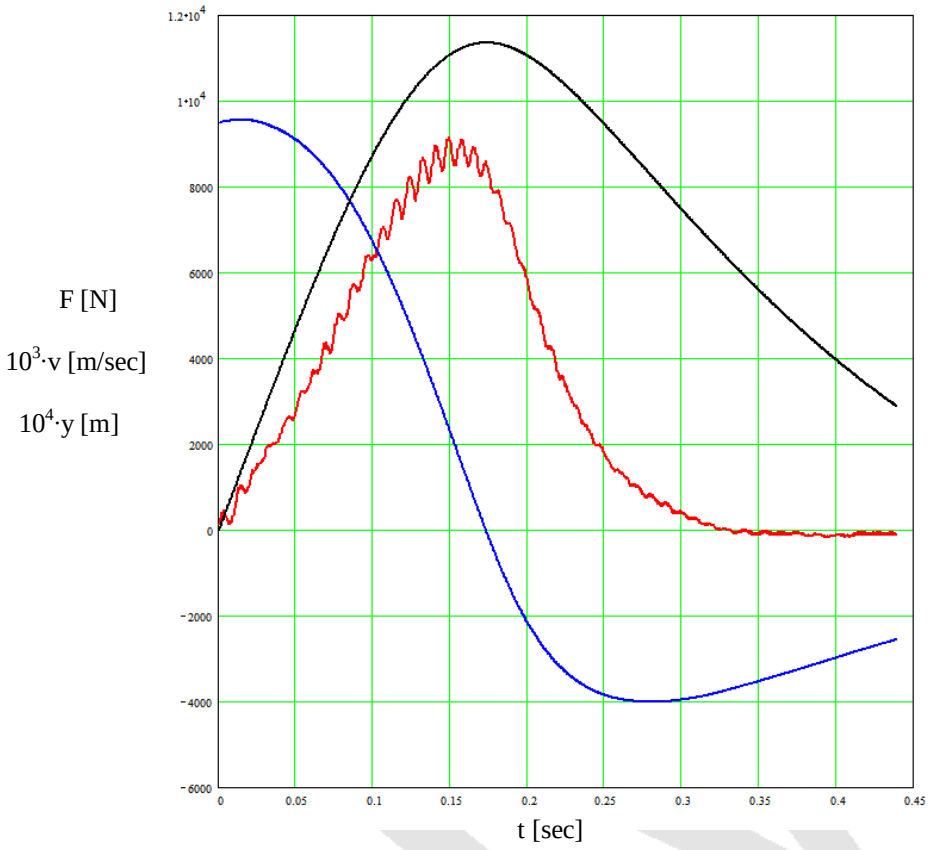


**Fig. 2.2.** F(t) in red, v(t) in blue and y(t) in black. The specific rope is the Edelrid Cobra climbing rope (10.3mm diameter), but the time behaviour of F is similar for all climbing ropes.

When F is plotted against y (Fig.2.3), one obtains a hysteresis loop, i.e. the rope shows different behaviour for stretching and un-stretching. The enclosed area of the hysteresis loop represents the dissipated energy into heat[3].

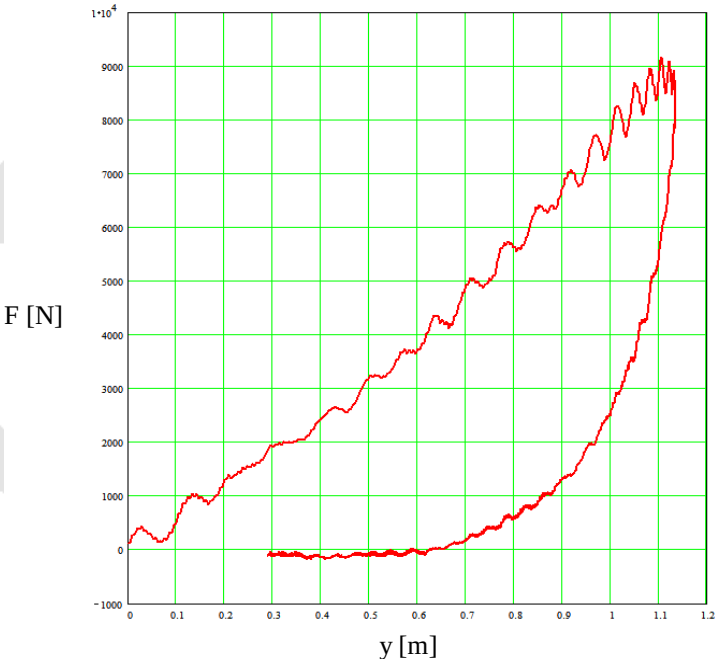


**Fig. 2.3.** Hysteresis between F and y.

## 3. Theoretical background

### 3.1 The linear SLS model

We first present in a mechanical formulation the so-called Standard Linear Solid Model (SLS) which is a common model for viscoelastic materials[4] including climbing ropes[5]. It is shown in Fig.3.1.

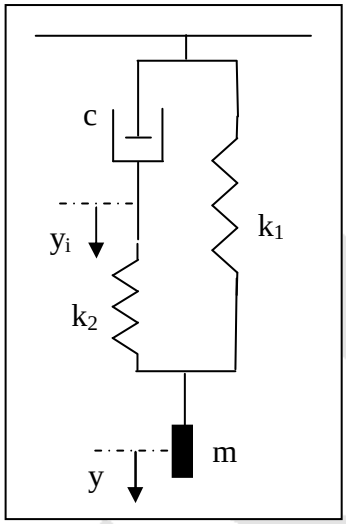


**Fig. 3.1.** SLS model (one of several equivalent forms of the model)

The model consists of two types of fibers. The first is pure elastic with a spring $k_1$, the second is described by the so-called Maxwell model (viscous damping c and spring $k_2$ in series). $y_i$ is an unobservable, inner friction variable.

The SLS model of Fig. 3.1 has

1. the kinetic energy $T = \frac{1}{2} m \dot{y}^2$ ,
2. the potential energy $V = \frac{1}{2} k_1 y^2 + \frac{1}{2} k_2 (y - y_i)^2 - mgy$ and
3. the dissipation function $D = \frac{1}{2} c \dot{y}_i^2$

Using the Lagrange function L = T - V and the Lagrange functions $\frac{d}{dt}\frac{\partial L}{\partial \dot{y}_i} = \frac{\partial L}{\partial y_i} - \frac{\partial D}{\partial \dot{y}_i}$ one obtains the equations of motion

$$m\ddot{y} + k_2 (y - y_i) + k_1 y = mg \qquad (3.1)$$

$$c\dot{y}_i + k_2 (y_i - y) = 0 \qquad (3.2)$$

D is responsible for the transformation of mechanical energy into dissipated (heat) energy $E_a$ given by

$$E_a(t) = \int_0^t c\dot{y}_i^2 dt \quad \text{or} \quad \frac{d(V+T)}{dt} = \frac{dU}{dt} = -2D \tag{3.3}$$

These equations are normally solved with the initial conditions

$$y_i(0) = 0,\ \dot{y}_i(0) = 0,\ y(0) = 0,\ \dot{y}(0) = v_0,\ \ddot{y}(0) = g\,.$$

Eliminating $y_i$ and introducing the relaxation time

$$\tau = c/k_2$$

and the spring constant

$k = k_1 + k_2$

one gets

$$\tau(m\dddot{y} + k\ddot{y}) + (m\ddot{y} + k_1\dot{y}) = mg \tag{3.4}$$

The static elongation $y_{stat}$ can be immediately read off as $mg/k_1$. The tension of the rope is $F = k_2(y - y_i) + k_1 y$ depending also on $y_i$.

The short time expansion for y(t) and F(t) using (3.4) is given by

$$y(t) = v_0 t + \frac{1}{2}gt^2 - \frac{1}{3!}v_0\frac{k}{m}t^3 + \frac{1}{4!}\left(v_0\frac{k_2^2}{mc} - g\frac{k}{m}\right)t^4 + O(t^5) \tag{3.5}$$

and

$$F(t) = mg - m\ddot{y}(t) = v_0 kt - \frac{1}{2}\left(v_0\frac{k_2^2}{c} - gk\right)t^2 + O(t^3) \tag{3.6}$$

In terms of viscoelastic theory, the SLS model consists of a Maxwell model described by $\dot{\sigma}_2/E_2 + \sigma_2/\eta = \dot{\varepsilon}$ and a parallel spring (Hooke's law) $\sigma_1 = E_1\varepsilon$. $\sigma$ is the stress and $\varepsilon$ is the strain. $E_{1,2}$ are the moduli of elasticity and $\eta$ is the viscosity which are both independent of the cross section q and the length L of the rope and can therefore be regarded as material constants. Because of $\sigma = \sigma_1 + \sigma_2$ one obtains

$$\dot{\sigma} + \frac{E_2}{\eta}\sigma - (E_1 + E_2)\dot{\varepsilon} - \frac{E_1E_2}{\eta}\varepsilon = 0 \tag{3.7}$$

This equation can be converted into (3.4) by the assignments

$$\sigma = \frac{1}{q}(mg - m\ddot{y}) = \frac{F}{q},\quad \varepsilon = y/L$$

$$c = \frac{q}{L}\eta \text{ and } k_{1,2} = \frac{q}{L}E_{1,2}$$

A different representation reveals the physical mechanism of the viscoelastic material. Integration of equation (3.2) and insertion into equation (3.1) yield:

$$m\ddot{y} + (k_1 + k_2)y - \frac{k_2^2}{c}\int_0^t \exp\left[\frac{-(t-t')}{\tau}\right] y(t')dt' = mg \qquad (3.8)$$

Thus the stress in the rope is not an instantaneous result of the momentary strain (like in the undamped case), but due to memory effects the full time history of the strain process in (3.8) contributes to the momentary stress.

In a phenomenological description one directly starts with a generalisation of the integral equation (3.8)

$$F(t) = H(0)y(t) + \int_0^t \dot{H}(t-t')y(t')dt' \qquad (3.9)$$

by choosing an appropriate memory kernel H, called the relaxation modulus. For (3.8), H is given by the simple

$$H(t) = H(\infty) + (H(0) - H(\infty))e^{-t/\tau} = k_1 + k_2 e^{-t/\tau} \qquad (3.10)$$

H(t) can be generalized in various ways[4], for example by a sum of exponential functions. But H(t) has to be always positive and monotonically decreasing, i.e. in the limit $t \to 0$ one gets $\dot{H}(t) \cong \dot{H}(0) \equiv \dot{H}_0 < 0$ and therefore

$$F(y) = H_0 y + \int_0^t \dot{H}(t-t')y(t')dt' \cong H_0 y - \left|\dot{H}_0\right|\int_0^t y(t')dt' = H_0 y - \left|\dot{H}_0\right|\int_0^\varepsilon y'\left|\frac{1}{v_0}\right|dy' = H_0 y - \left|\frac{\dot{H}_0}{v_0}\right|\frac{y^2}{2} \qquad (3.11)$$

Thus, for a general class of viscoelastic models and for small y the tension F is given by an elastic part $H_0 \cdot y$ followed by a negative dissipative term of second order in y which is responsible for a negative curvature of F(y). As a consequence positive or zero curvature implies that no damping exists.

## 4. Special SLS cases

We now discuss some important special cases of the SLS with analytical solutions. Furthermore, an exact solution of the SLS model at its critical point (where the oscillatory solutions just disappear) is found in the Appendix.

### 4.1. The undamped harmonic oscillator (HO)

One gets the undamped harmonic oscillator (HO) from (3.4) for c = 0 ($k = k_1$) as well as for $c \to \infty$ with spring constant $k = k_1 + k_2$:

$$m\ddot{y} + ky = mg \tag{4.1}$$

This equation has to be solved with the initial conditions $v(0) = v_0$ and $y(0) = 0$. The solution is:

$$y(t) = \frac{v_0}{\omega}\sin(\omega t) + \frac{g}{\omega^2}(1 - \cos(\omega t)) \tag{4.2a}$$

or equivalently

$$y(t) = \frac{g}{\omega^2} + \frac{1}{\omega^2}\sqrt{v_0^2 \cdot \omega^2 + g^2}\,\sin\left(\omega t - \arctan(\frac{g}{v_0\omega})\right) \tag{4.2b}$$

with $\omega = \sqrt{\frac{k}{m}}$ .

The maximum elongation occurs at time $t_2 = \frac{1}{\omega}\left(\frac{\pi}{2} + \arctan\left(\frac{g}{v_0\omega}\right)\right)$ and is given by

$$y_{max} = \frac{g}{\omega^2} + \frac{1}{\omega^2}\sqrt{v_0^2 \cdot \omega^2 + g^2}\ . \tag{4.3}$$

A fall of the height h results in a fall velocity $v_0 = \sqrt{2gh}$ of the mass m.

With the modulus of elasticity $E = L \cdot k/q$ one gets the well-known formula[6] for the maximum rope tension $F_{max} = ky_{max}$ which occurs at $t_1$ which is equal to $t_2$ in the case of the HO:

$$F_{max} = mg + m\sqrt{v_0^2 \cdot \omega^2 + g^2} = mg + \sqrt{2ghmk + m^2g^2} = mg + \sqrt{2mgEqf + m^2g^2} \tag{4.4}$$

using the already introduced fall factor f=h/L. Because E is a material constant, $F_{max}$ only depends on the fall factor f. For constant f, an increasing fall energy mgh is compensated by the rope which becomes less stiff when L increases. The duration of the impact is approximately given by $t_2 \cong \sqrt{\frac{mL}{Eq}}\frac{\pi}{2}$ independent of $v_0$.

On the one side the angular frequency ω can be calculated from the static elongation $y_{stat}$ by $\omega_{stat} = \sqrt{\frac{g}{y_{stat}}}$, but on the other side from (4.4), $\omega = \frac{1}{mv_0}\sqrt{F_{max}(F_{max} - 2mg)}$. If the HO model would be valid, both ω would be equal. For our specific climbing rope with a relative $y_{stat}/L \approx 7\%$, however, one obtains $\omega_{stat} = 6.7\,\mathrm{sec}^{-1}$ and $\omega = 10.8\,\mathrm{sec}^{-1}$ showing the deficiencies of the HO.

Elimination of the spring constant k from equation (4.8) by means of $k = F^{max}/y^{max}$ yields

$$F^{max} = 2mg\frac{h + y^{max}}{y^{max}} = 2mg + \frac{mv_0^2}{y^{max}} \tag{4.5}$$

expressing energy conservation. Independent of any material parameter, this relation between $F_{max}$ and $y_{max}$ should be valid for all ropes, but it is not observed in reality.

### 4.2. The Maxwell and Kelvin models

The Maxwell model appears from the SLS model for $k_1 = 0$. It is a good approximation of the SLS model for small times and has an exact analytical solution. Because of the lacking $k_1$ it cannot describe the long time properties of the SLS.

With the already introduced terms $\omega_2^2 = k_2/m$ and $\kappa = k_2/2c$ equations (3.1) and (3.2) are now:

$$\ddot{y} + \omega_2^2(y - y_i) = g \tag{4.6}$$
$$\dot{y}_i - 2\kappa(y - y_i) = 0 \tag{4.7}$$

With the new variable $z = y - y_i$, one obtains its equation of motion

$$\ddot{z} + 2\kappa\dot{z} + \omega_2^2 z = g \tag{4.8}$$

F can also be expressed by z

$$F = mg - m\ddot{y} = m\omega_2^2 z \tag{4.9}$$

For the elongation y(t) follows

$$y(t) = z(t) + y_i(t) = z(t) + \int_0^t \dot{y}_i(t)dt = z(t) + 2\kappa\int_0^t z(t)dt \tag{4.10}$$

The exact solution of (4.9) is given by

$$z(t) = \frac{g}{\omega_2^2}\left(1 - e^{-\kappa t}\cos(\Omega t) - \frac{\kappa}{\Omega}e^{-\kappa t}\sin(\Omega t)\right) + e^{-\kappa t}\left(\frac{v_0}{\Omega} - \frac{\kappa g}{\omega_2^2\Omega}\right)\sin(\Omega t) \tag{4.11}$$

using the initial conditions $\dot{z}(0) = v_0$ and $z(0) = 0$ and with $\Omega^2 = \omega_2^2 - \kappa^2$. An approximation correct up to first order in the small parameters $\kappa/\omega_2$ and $\frac{g}{v_0\omega_2}$ reduces z(t) from (4.11) to

$$z(t) \cong \frac{g}{\omega_2^2}\left(1 - e^{-\kappa t}\cos(\omega_2 t)\right) + e^{-\kappa t}\frac{v_0}{\omega_2}\sin(\omega_2 t) \tag{4.12}$$

The time of the maximum z-elongation is $t_1 \cong \frac{1}{\Omega}\left(\arctan\left(\frac{\Omega}{\kappa - g/v_0}\right)\right) \approx \frac{1}{\omega_2}\left(\frac{\pi}{2} - \frac{\kappa}{\omega_2} + \frac{g}{v_0\omega_2}\right)$.

To first order in $\kappa/\omega_2$ we get the maximum tension

$$F_{max} = m\omega_2^2 z_{max} = mg + m\sqrt{v_0^2\omega_2^2 e^{-\frac{\pi\kappa}{\omega_2}} + g^2} \qquad (4.13)$$

From energy conservation the absorbed energy is given by

$E_a(t) = \frac{1}{2}mv_0^2 - \left(\frac{1}{2}m\omega_2^2 z^2 - mgy_2(t) + \frac{m}{2}\dot{z}^2\right)$. Neglecting the small influence of g, i.e. using $z(t) \cong e^{-\kappa t}\frac{v_0}{\omega_2}\sin(\omega_2 t)$, we obtain for $\kappa/\omega_2 << 1$ the well-known result of the damped harmonic oscillator:

$$E_a(t) = E_0\left(1 - e^{-2\kappa t}\right) \qquad (4.14)$$

The Kelvin model is obtained from (3.4) in the limit $k_2 \to \infty$:

$$m\ddot{y} + c\dot{y} + k_1 y = mg \qquad (4.15)$$

which is the same equation as (4.8) taking into account the changed parameters. The initial conditions are the same, so (4.11) is also the solution of (4.15).
At the beginning of the rope stretch (t=0), friction causes a discontinuous change of $cv_0$ in the tension which is not observed for climbing ropes.

## 5. Time-delayed friction and adiabatic stretching

We are now prepared to discuss the experiments from chapter 2.
In these experiments F(y) linearly increases for small y (Fig.2.3). This is consistent with the general result (3.11) for the tension $F \cong H_0 y - \left|\dot{H}_0/2v_0\right| y^2$ for small y. The linear elastic part $H_0 y$ is now determined from the experimental F(y) by linear regression and then subtracted from F. The resulting dissipative remainder $F - ky$ (we use the more common spring constant k instead of $H_0$) is compared with the Kelvin model, the HO and the SLS model in Fig.5.1.

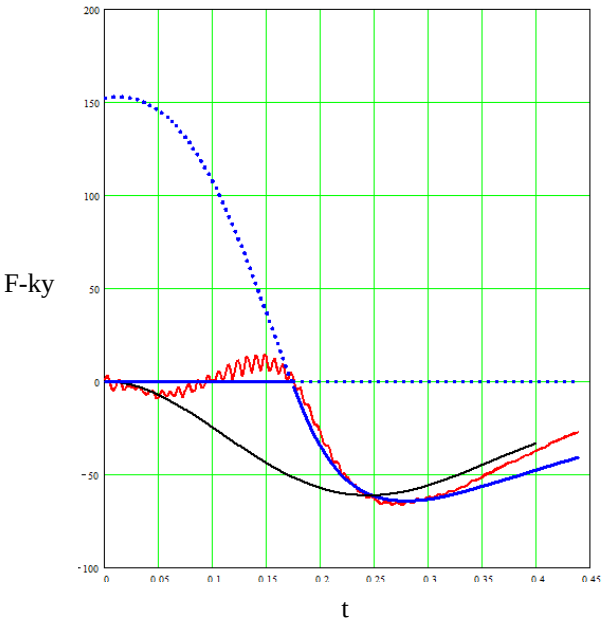


**Fig. 5.1.** The measured F-ky with $\omega = \sqrt{k/m} = 9.5\text{sec}^{-1}$ (red curve). The regression range for the determination of the initial slope $m\omega^2$ is chosen between 0<y<0.8m in order to take into account a part of the nonlinear tension. F-ky of the Kelvin model (dotted for $t< t_1$) and of the HO (dotted for $t>t_1$) are shown in blue. The black curve represents the SLS model.

None of the models can explain the measured $F - ky$ . But it is striking that the frictionless HO for $t<t_1$ together with the Kelvin model for $t>t_1$ is a surprisingly good combination suggesting that there is little or no friction for $t<t_1$. There are two further indications of time-delayed friction.
For larger elongations, as already mentioned dissipation leads to a negative curvature of F in contrast to the measured F, which has a positive curvature almost up to $F_{max}$ .
Furthermore, friction is responsible for a time difference $\Delta t = t_2 - t_1$ between the times of the force and elongation maxima. The very small experimental value of $\Delta t/t_1 = 0.157$ also indicates low friction until the force maximum is reached.
To explain this time-delayed friction we consider the thermal properties of the rope.
The first law of thermodynamics $dU = dQ + Fdy$ states that the change of the internal energy dU of a system is given by the added heat dQ and added work Fdy=kydy done on the system. It is furthermore assumed that $U = C_L T$ is only a function of temperature with the specific heat at constant length $C_L = (\partial U/\partial T)_L$ .
Statistical mechanics elastomer models [7,8] lead to a linear temperature dependence of the spring constant $k(T) = \alpha T$. This temperature dependence is the reason for the contraction of an elastomer when heated in contrast to most other materials.
During stretching under isothermal conditions, work Fdy>0 is done on the rope and therefore heat flows outwards (dQ<0). In the fall experiment, however, there are no isothermal equilibrium conditions because the rope is stretched very fast. Rather, adiabatic conditions prevail without immediate heat exchange with its surroundings, i.e. $dQ \cong 0 = C_L\, dT/T - \alpha y dy$ .

Integrating this equation, one gets a temperature increase from $T_0$ to $T_1 = T_0 \exp(\alpha y_{max}^2 / 2C_L)$. For elastomers like rubber bands this temperature increase is well known and can be tested easily by stretching a rubber band using the lips as a temperature sensor.
All the work which was done by stretching the rope is now reversibly stored in its internal energy $U = C_L(T_1 - T_0)$. But because of the temperature difference, there must be eventually a heat and entropy exchange with the surroundings. This exchange process starts with a time-delay near the maximum of the force $F_{max}$ and can be viewed approximately as a jump from $F_{max}$ to a lower force almost at constant length (dL=0). No work is done, i.e. FdL = 0, but heat $Q = -U = C_L(T_0 - T_1) < 0$ is flowing outward. Together with a second adiabate for the rest of the motion, the stretching-unstretching process of the rope is reminiscent of a part of an Otto cycle (Fig.5.3)[9].

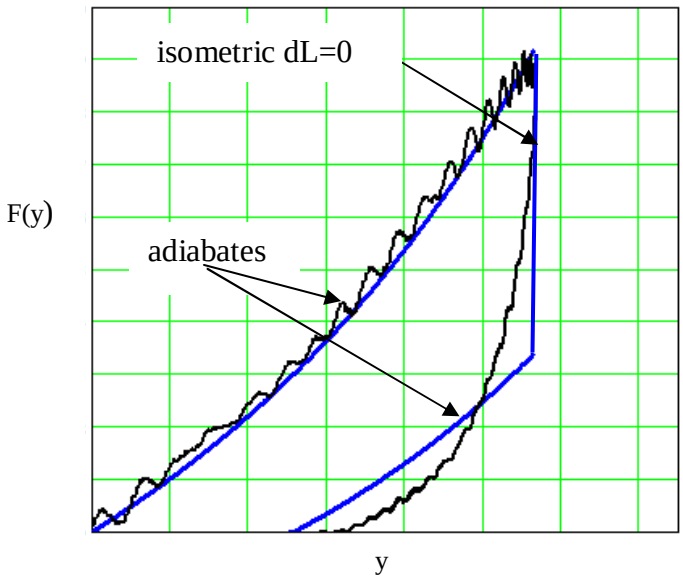


**Fig.5.3.** Hysteresis as a thermodynamic process approximated by an Otto cycle (blue).In contrast to an isothermal process with a linear force one has an adiabatic process with a nonlinear force $F \propto y \exp(\alpha y^2 / 2C_L)$. There is a strong drop in F almost at constant length where heat exchange with the surroundings takes place.

## 6. Models with time-delayed friction

### 6.1. The linear Kelvin model

We have shown that two regions with and without friction can be distinguished, so that the Kelvin model can be described piecewise by

$$\begin{aligned} &\ddot{y} + \omega_1^2 y = g && \text{for } t \le t_1 \\ &\ddot{y} + 2\delta\dot{y} + \omega_1^2 y = g && \text{for } t > t_1 \end{aligned} \qquad (6.1a)$$

with $\omega_1 = \sqrt{k_1/m}$, $\delta = c/2m$ and $t_1 = \frac{1}{\omega_1}\left(\frac{\pi}{2} + \arctan\left(\frac{g}{v_0\omega_1}\right)\right)$. With the step function $\Phi$ a more compact notation of (6.1a) is possible:

$$\ddot{y} + 2\delta\dot{y}\Phi(-\dot{y}) + \omega_1^2 y = g \qquad (6.1b)$$

The initial conditions and the conditions at time $t_1$ are

$$y(0) = 0, \quad y(t_1) = \frac{g}{\omega_1^2} + \frac{1}{\omega_1^2}\sqrt{v_0^2 \cdot \omega_1^2 + g^2}, \quad v(0) = v_0, \quad v(t_1) = 0 \qquad (6.2)$$

The solution for $t \le t_1$ is given by (4.2) and the solution for $t > t_1$ can also be easily calculated with the result

$$y(t) = \left(y(t_1) - \frac{g}{\omega_1^2}\right)\left(\delta\frac{\sin(\Omega_1(t-t_1))}{\Omega_1} + \cos(\Omega_1(t-t_1))\right)e^{-\delta(t-t_1)} + \frac{g}{\omega_1^2} \qquad (6.3)$$

with $\Omega_1 = \sqrt{\omega_1^2 - \delta^2}$. The static case is the same as for the HO.
Because we are close to the aperiodic limit $\omega_1 = \delta$, this solution is also given for $t>t_1$

$$y(t) = \left(y(t_1) - \frac{g}{\delta^2}\right)((t-t_1)\cdot\delta + 1)e^{-\delta(t-t_1)} + \frac{g}{\delta^2} \qquad (6.4)$$

The tension $F = mg - m\ddot{y}$ is obtained simply by differentiating (6.4) twice and describes a relaxation process into equilibrium for $t>t_1$ approximately given by

$$F(t) \cong F_{max}e^{-2\delta(t-t_1)}$$

with a relaxation time of $1/2\delta$. In Fig.6.1 the theoretical F is compared with the data. The cusp seen in this figure comes from the spontaneous onset of friction at $t_1$. The energy absorption rate is given by $\dot{E}_a(t) = 2\delta m\dot{y}^2\Phi(t - t_1) \cong 2\delta m v_0^2[\delta(t - t_1)]^2 e^{-2\delta(t-t_1)}\Phi(t - t_1)$ and occurs on a time scale of $1/\delta$.

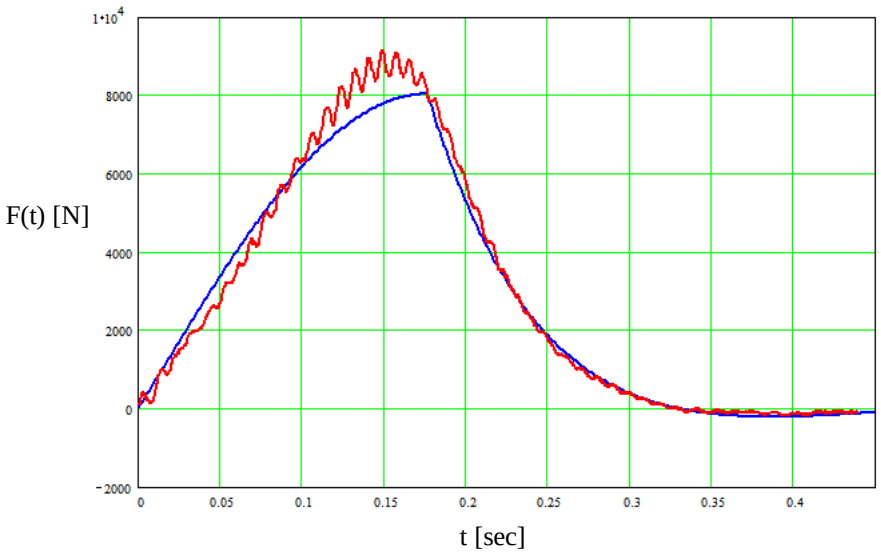


**Fig.6.1.** F as a function of t. The experimental curve in red, the theoretical one calculated from (6.4) with $\delta=\omega_1=9.5\text{sec}^{-1}$ in blue.

## 6.2. The nonlinear Duffing oscillator

As seen from Fig.6.1 the stiffness of the rope increases for larger deformations which cannot be explained by a linear F(y). A statistical physics approach leads to a more general F(y) for elastomers valid also for large deformations. In this approach, tension is related to elongation by the Langevin function $\bar{L}$ [16] which has the expansion $F(y) \propto \bar{L}^{-1}(y) = ky + k_3 y^3 + O(y^5)$ with a force term proportional to $y^3$ after the linear term. An additional $y^3$-contribution to the force comes from the adiabatic process. We neglect the change of this force term due to the nonadiabatic backward motion of the rope.

Adding the nonlinear term $\omega_3^2 y^3$ to the equations (6.1) we obtain

$$\ddot{y} + 2\delta\dot{y}\Phi(-\dot{y}) + \omega_1^2 y + \omega_3^2 y^3 = g \qquad (6.5)$$

called the Duffing oscillator.

The rope tension is given by $F = k_1 y + k_3 y^3 + 2m\delta\dot{y}\Phi(-\dot{y})$ with the nonlinear force constant $k_3 = m\omega_3^2$. The step function $\Phi$ at $t_1$ where $\dot{y}$ changes its sign could be replaced by a smoother version of $\Phi$. That would lead to a slightly better fit without the small cusp at $F(t_1)$ but also to an unnecessarily more complicated model.

The equation (6.5) allows the determination of the parameters $\omega_1$ and $\omega_3$ for times $t < t_1$ by regression methods. Once $\omega_1$ and $\omega_3$ are known, the conservative force $k_1 y + k_3 y^3$ can be separated and the friction force $2\delta\dot{y}\Phi(-\dot{y})$ is immediately obtained. All forces are shown in Fig.6.2.

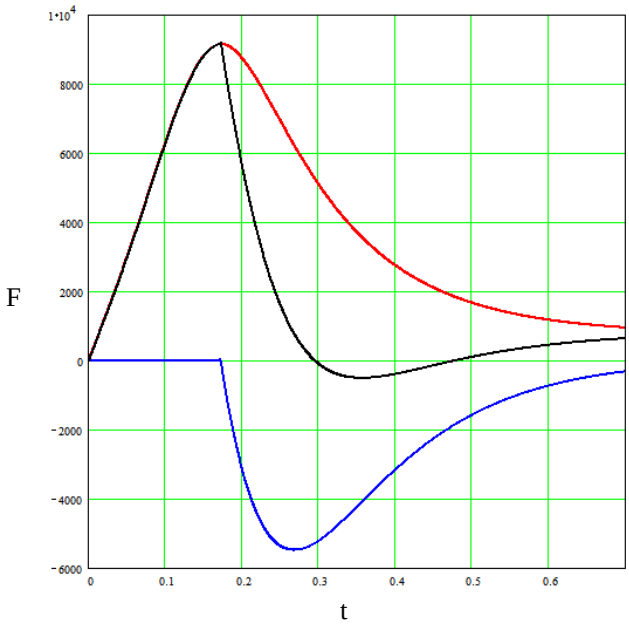


**Fig.6.2**. The rope tension F (black) as the sum of the elastic force (red) and the friction force (magenta).

The numerical solution of equation (6.5) is presented in the next Fig.6.3. In Fig.6.4, a comparison between the calculated and experimental hysteresis of F and y is shown.

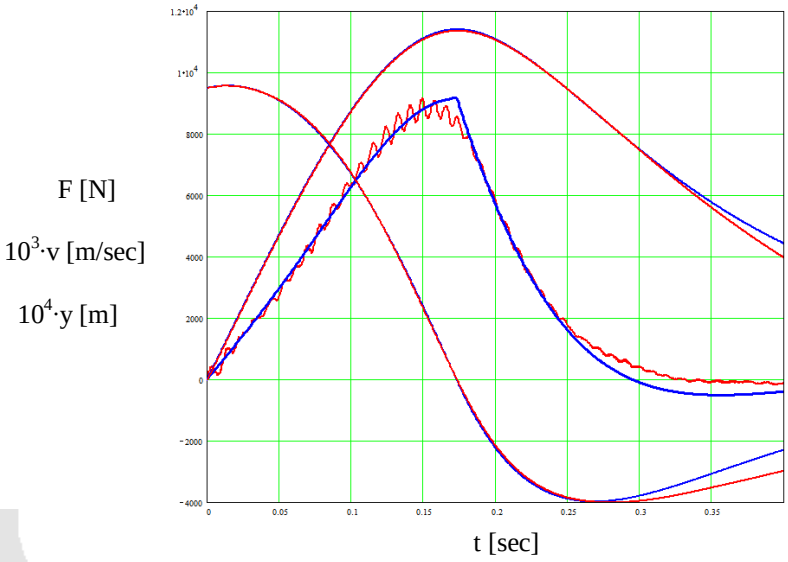


**Fig.6.3.** The rope tension F, the elongation y and the velocity v calculated by (6.5) in blue compared with the corresponding measured F,y,v in red. The parameters are $\omega_1$=8.6sec$^{-1}$, $\omega_3$=4.5(m·sec)$^{-1}$, $\delta$=8.6sec$^{-1}$. Friction begins at $t_1$, determined by $v(t_1)=0$. Without $\omega_3$, the damped oscillator would be exactly at its critical damping point with the fastest possible approach to the rest position.

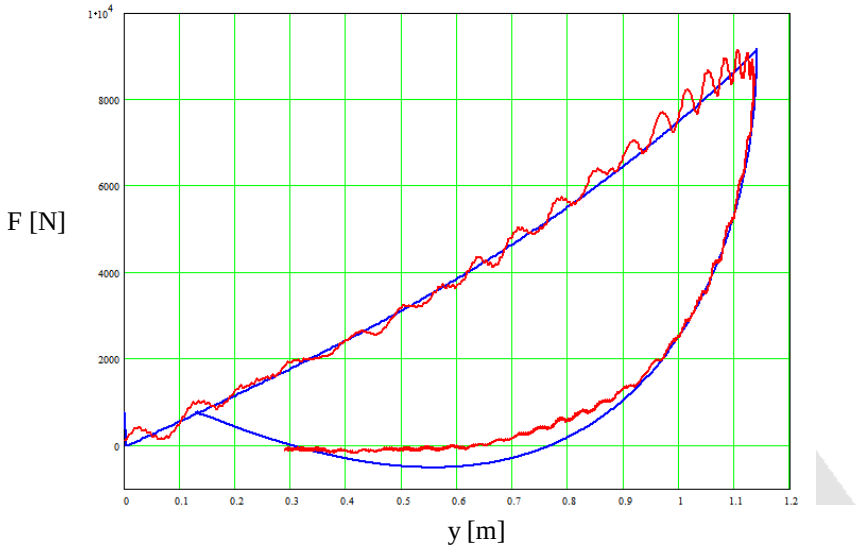


**Fig.6.4.** Comparison between the calculated (6.5) and experimental hysteresis of F and y.

Multiplying the friction force by the velocity $\dot{y}(t)$, one obtains the energy absorption rate $\dot{E}_a(t)$. Note, that $\dot{E}_a(t)$ depends on the underlying model. For the SLS model with its internal friction variable it has to be calculated differently. In Fig.6.5 a comparison with the theoretical rate $\dot{E}_a(t) = 2\delta m\dot{y}^2\Phi(-\dot{y})$ is shown.

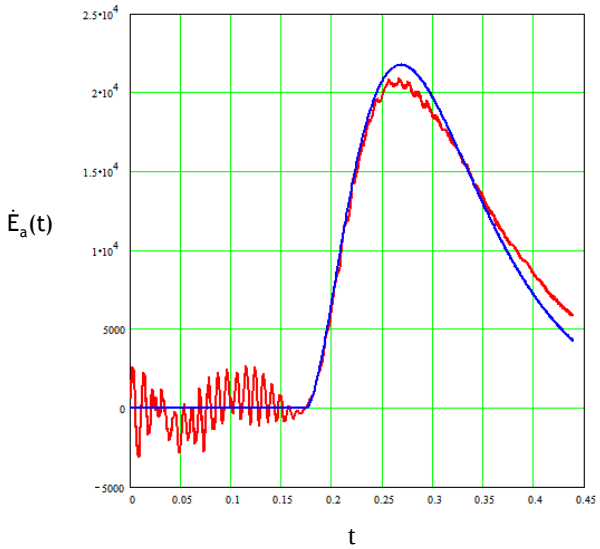


**Fig.6.5.** Comparison between the measured and calculated energy absorption rate.

The above calculations have been performed also for the Beal Joker rope which is known as a rather soft rope ($F_{max}$= 8.1kN, $y_{max}$=1.36m) different from the Edelrid Cobra.
The agreement with the measured F(t) is as good as for the Edelrid Cobra but with changed parameters as seen in the following table.

| | $\omega_1[sec^{-1}]$ | $\omega_3\,[m^{-1}\cdot sec^{-1}]$ | $\delta[sec^{-1}]$ | $\omega_3/\,\omega_1[m^{-1}]$ |
|---|---|---|---|---|
| Edelrid Cobra 10.3 | 8.6 | 4.5 | 8.6 | 0.523 |
| Beal Joker 9.1 | 7.1 | 3.7 | 7.4 | 0.521 |

Note that the ratio of $\omega_3/\,\omega_1$ are the same for both ropes.

The static elongation of the Duffing oscillator is only slightly different from the linear case and thus given by $y_{stat} = g/\omega_1^2$ . With the above $\omega_1$=8.6sec$^{-1}$ one obtains a relative static elongation of 5%. This value is not far from the observed one of about 7%.

### 6.3. **The nonlinear $F_{max}$**

In the fall experiments of[10] the fall factor f and the mass m have been varied independently from each other. The HO impact formula for $F_{max}$ (4.4) written as

$$\frac{F_{max}}{m} = g + \sqrt{2gEq\frac{f}{m} + g^2} \tag{6.6}$$

is only a function of the ratio f/m. If this formula would be correct, all measurements represented by circles in Fig.6.6 would lie on one curve. However, $F_{max}/m$ is a function of both f and m, and a whole family of curves emerge. The numerical calculation of $F_{max}$ from (6.5) is also shown in Fig.6.6 and is in agreement with the data.

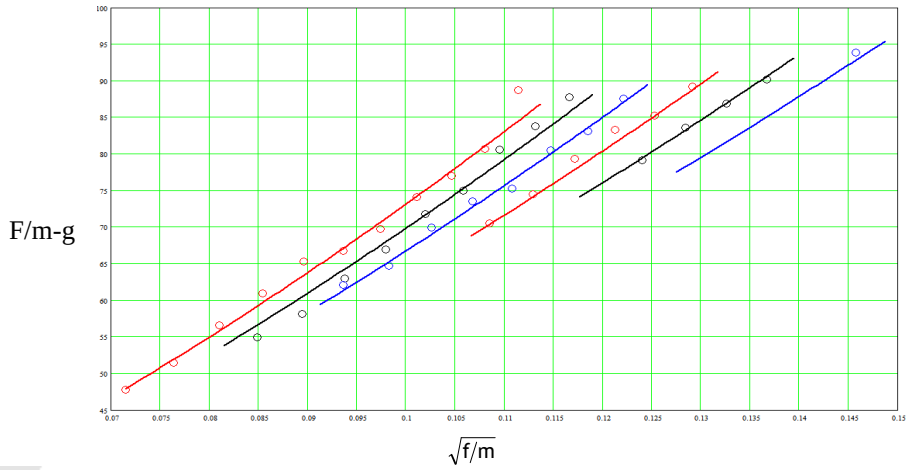


**Fig.6.6.** Measured (circles) and calculated F/m-g as a function of $\sqrt{f/m}$.
The masses vary from m=80kg (blue), m=91kg(black), m=102kg(red), m=114kg(blue), m=125kg(black), m=137kg(red).

In the following an analytic approximation of $F_{max}$ and $y_{max}$ for g > 0 is given. Note that an exact solution is possible for g=0. Energy conservation and the definition of $F_{max}$ lead to

$$\frac{1}{2}v_0^2 + gy_{max} = \frac{\omega_1^2}{2}y_{max}^2 + \frac{\omega_3^2}{4}y_{max}^4 \tag{6.7a}$$

$$\frac{F_{max}}{m} = \omega_1^2 y_{max} + \omega_3^2 y_{max}^3 \tag{6.7b}$$

The solution of (6.7a) for a linear force is already known and its first order approximation in g is given by

$$y_{max}^{0} = \frac{g}{\omega_1^2} + \frac{1}{\omega_1^2}\sqrt{v_0^2 \cdot \omega_1^2 + g^2} \cong \frac{g}{\omega_1^2} + \frac{v_0}{\omega_1}$$

Looking for a solution of (6.7a) which is correct to first order in g and $\omega_3^2$ with the ansatz

$$y_{max} \cong \frac{v_0}{\omega_1} + Ag + B\omega_3^2 \tag{6.8}$$

one obtains after collecting all terms of O(g) and O($\omega_3^2$) $B = -\frac{1}{4}\frac{v_0^3}{\omega_1^5}$ and $A = \frac{1}{\omega^2} - \omega_3^2\frac{v_0^2}{\omega^6}$.

$y_{max}$ from (6.8) with A and B is now inserted into the following expression:

$$(F_{max} - mg)^2 = (m\omega^2 y_{max} + m\omega_3^2 y_{max}^3 - mg)^2 = \Omega^2 m^2 v_0^2 \tag{6.9}$$

$\Omega^2$ is chosen such that the correct form of linear $F_{max}$ is preserved. Its solution is given by

$$\Omega^2 = \omega_1^2 + \frac{3}{2}\frac{\omega_3^2 v_0^2}{\omega_1^2} + 4g\omega_3^2\frac{v_0}{\omega_1^3} + O(\omega_3^4) + O(g^2) \tag{6.10}$$

Ω agrees with the exact solution for g = 0 in second order of $\omega_3$. Furthermore, it depends on the amplitude $v_0/\omega_1$, typical for nonlinear systems.

Using $qE_3 = mL^3\omega_3^2$ and $qE_1 = mL\omega_1^2$ we get for $F_{max}$

$$F_{max} = mg + m\sqrt{v_0^2 \cdot \Omega^2 + g^2} \cong mg + m\sqrt{v_0^2\frac{qE_1}{Lm}\left(1 + \frac{3}{2}\left(\frac{m}{q}\right)\frac{E_3}{E_1^2}\frac{v_0^2}{L} + 4g\left(\frac{m}{q}\right)^{\frac{3}{2}}\frac{E_3}{E_1^{5/2}}\frac{v_0}{L^{1/2}}\right) + g^2} \tag{6.11a}$$

resp.

$$\frac{F_{max}}{m} \cong g + \sqrt{2g\frac{f}{m}qE_1\left(1 + \frac{3}{2}\left(\frac{1}{q}\right)m^2\frac{E_3}{E_1^2}2g\frac{f}{m} + 4g\left(\frac{1}{q}\right)^{\frac{3}{2}}m^2\frac{E_3}{E_1^{5/2}}\sqrt{2g\frac{f}{m}}\right) + g^2} \tag{6.11b}$$

Because of the terms $m^2\frac{f}{m}$ and $m^2\sqrt{\frac{f}{m}}$, $F_{max}/m$ is no longer a function of f/m alone leading to a set of the curves seen in Fig.6.6.
In Fig.6.7 the approximation (6.11) is compared with the exact solution for $F_{max}$ for 3 different masses 80kg, 100kg and 120kg as a function of the fall factor f. The relative error is always smaller than 8%.

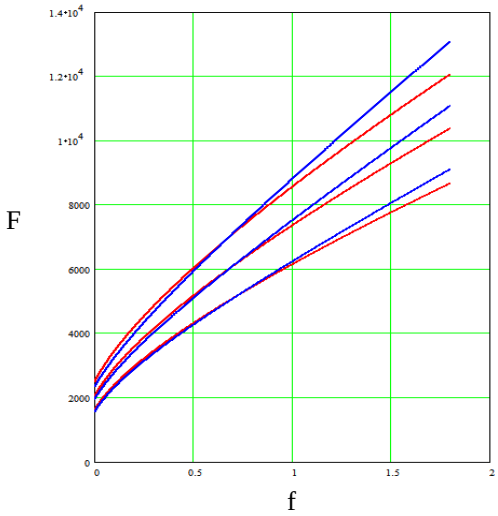


**Fig.6.7.** Comparison between the exact $F_{max}$ (red curves) and its approximation (6.11) in blue as a function of the fall factor f for different masses m = 80kg, 100kg and 120kg.

## 7. Elastic continuum description of the rope

So far the mass $m_{rope}$ of the climbing rope has been neglected. In this chapter it is shown that $m_{rope}$ is responsible for the small oscillatory motions of F(t).
Starting with a discrete description, we use the equations of motions of a linear chain of n small masses μ without friction and a spring constant $\bar{k}$ between two small masses (Fig.7.1)

$$\begin{aligned}
&\mu\ddot{u}_1 + \bar{k}u_1 + \bar{k}(u_1 - u_2) = \mu g \\
&\mu\ddot{u}_2 + \bar{k}(u_2 - u_1) + \bar{k}(u_2 - u_3) = \mu g \\
&\dots \\
&\mu\ddot{u}_i + \bar{k}(u_i - u_{i-1}) + \bar{k}(u_i - u_{i+1}) = \mu g \\
&\dots \\
&(m+\mu)\ddot{u}_n + \bar{k}(u_n - u_{n-1}) = (m+\mu)g
\end{aligned} \qquad (7.1)$$

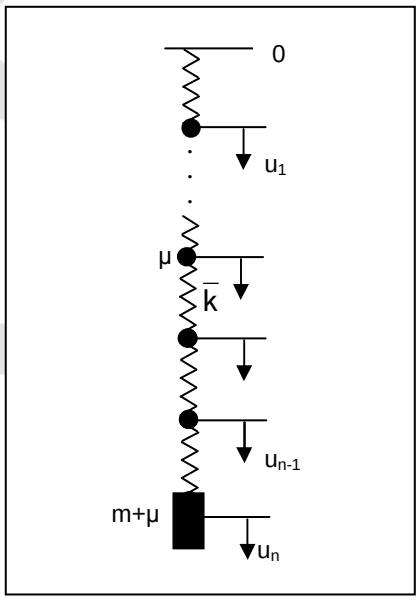


**Fig.7.1.** Part of a linear chain of small masses μ with a large mass m at the end at position n.

For μ = 0 the old HO equation $m\ddot{u}_n + \frac{\bar{k}}{n}u_n = mg$ is regained with $u_n(t)=y(t)$, the spring constant $k = \bar{k}/n$ of n serial connected springs with $\bar{k}$. In the continuum limit $u_{n+1} - u_n \to \frac{\partial u(x,t)}{\partial x}$ we get from (7.1) the elastic wave equation

$$\ddot{u}(x,t) - c_s^2 \frac{\partial^2 u(x,t)}{\partial x^2} = g \tag{7.2}$$

for longitudinal oscillations with the velocity of sound $c_s = \sqrt{E/\rho}$, the mass density $\rho = \frac{m_{rope}}{Lq}$ and the mass of the rope $m_{rope} = n\mu$. At x = L the continuum form of the last equation of (7.1) for u(L,t) (= y(t)) is given by

$$\ddot{u}(L,t) + \frac{Eq}{m}\frac{\partial u(L,t)}{\partial x} = g \tag{7.3}$$

Neglecting g and looking for oscillatory solutions with the separation ansatz u(x,t) = X(x)T(t) for (7.2) one obtains $\frac{1}{X(x)}X''(x) = \frac{1}{c_s^2}\frac{1}{T(t)}\ddot{T}(t) = -\kappa^2$ and together with (7.3)

$$\frac{\ddot{T}(t)}{T(t)} = -\frac{Eq}{m}\frac{X(L)'}{X(L)} = -\kappa^2 c_s^2 \tag{7.4}$$

The general solution of X(x) is given by $X = C_1\cos(\kappa x) + C_2\sin(\kappa x)$. From the fixed end boundary condition X(0) = 0, X must be of the form $X = C_2\sin(\kappa x)$ so that from (7.4) one has the equation

$$\kappa L\tan(\kappa L) = \frac{m_{rope}}{m} \tag{7.5}$$

with the first two solutions $\kappa_1 \approx \frac{1}{L}\sqrt{\frac{m_{rope}}{m}}$ and $\kappa_2 \approx \frac{\pi}{L} + \frac{m_{rope}}{m\pi L} \approx \frac{\pi}{L}$. From the dispersion relation for sound waves the frequency

$$\omega_1 = c_s\kappa_1 = \sqrt{\frac{E}{\rho}}\frac{1}{L}\sqrt{\frac{m_{rope}}{m}} = \sqrt{\frac{Eq}{mL}} \tag{7.6}$$

follows. Thus the $\kappa_1$ mode describes the already known oscillation of the large mass m with the frequency of the simple HO. The $\kappa_2$ mode with frequency

$$\omega_2 = \sqrt{\frac{E}{\rho}}\frac{\pi}{L} \tag{7.7a}$$

describes the fast oscillation of the rope seen in Fig.7.2 and Fig.7.3 and depends only on the properties of the rope. The ratio

$$\frac{\omega_2}{\omega_1} = \pi\sqrt{\frac{m}{m_{rope}}} \tag{7.7b}$$

with $m_{rope}$ = 177g (Edelrid Cobra) can be compared with the measurements. From the initial slope of F(y) we get $\omega_1 = 8.6\,\mathrm{sec}^{-1}$, so that equation (7.7b) gives $\omega_2 = 574\,\mathrm{sec}^{-1}$. The measured frequency of the $\kappa_2$ mode for small times is $\hat{\omega}_2 = 580\,\mathrm{sec}^{-1}$ in excellent agreement with the theoretical result (Fig.7.2).

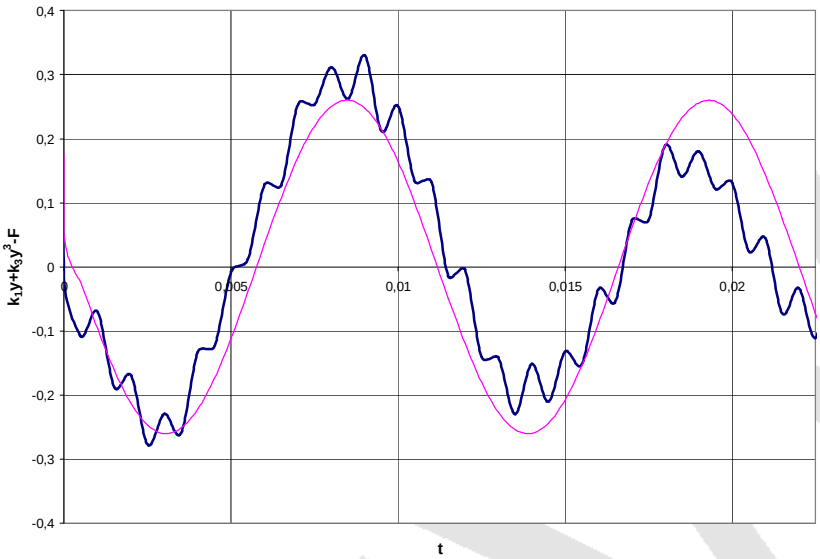


**Fig.7.2.** The second mode oscillation of the residuum $k_1y + k_3y^3 - F$ at the beginning of the fall with an angular frequency (blue curve) of 580 $sec^{-1}$. Note that also the third mode is visible.

Near the force maximum $F_{max}$, the measured fast oscillation, given by $\hat{\omega}_2^{F\,max} = 740\,\mathrm{sec}^{-1}$, is increased by about 27.5% relative to $\hat{\omega}_2$ for small elongations (Fig.7.3).

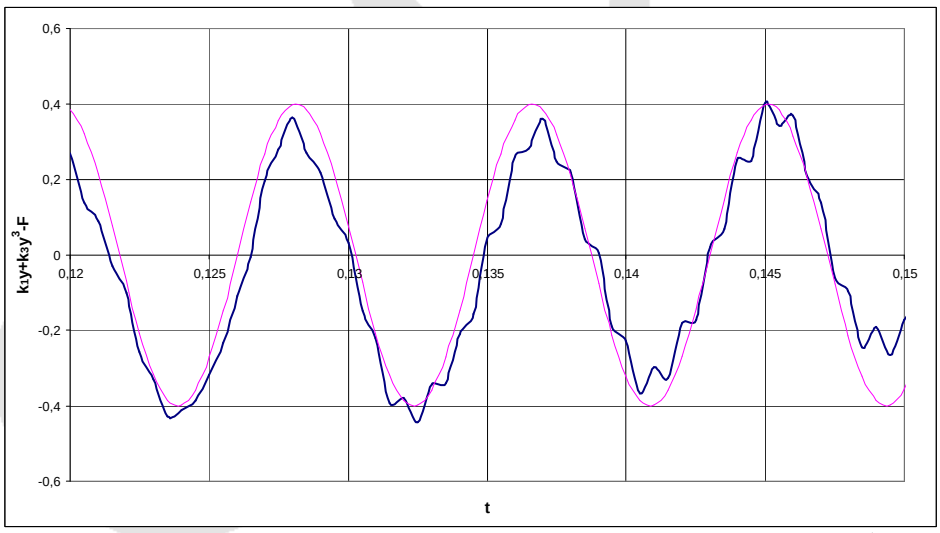


**Fig.7.3.** The second mode near $F_{max}$ with an angular frequency of 740 $sec^{-1}$.

This can also be explained by the nonlinear model. The changed frequency at $F_{max}$ is

$$\Omega = \omega_1 \sqrt{1 + \frac{3}{2}\frac{\omega_3^2 v_0^2}{\omega_1^4} + 4g\omega_3^2 \frac{v_0}{\omega_1^5}}$$

from equation (6.10) which has to be used instead of $\omega_1$ and yields a relative frequency increase of $\frac{\Omega}{\omega_1} - 1 \sim 29\%$ , again in excellent agreement with the experimental value.
Finally, we present without calculation the result of $\ddot{u}(L,t)$ for small $m_{rope}/m$

$$\ddot{u}(L,t) = \ddot{y}(t) \cong -v_0\omega_1 \sin(\omega_1 t) - \frac{3}{\pi} v_0 \omega_1 \sqrt{\frac{m_{rope}}{m}} \sin\left(\pi\omega_1 \sqrt{\frac{m}{m_{rope}}} t\right)$$

with an amplitude ratio of $\frac{3}{\pi}\sqrt{\frac{m_{rope}}{m}} \cong 0.045$ that is also conform with the experimental data.

## 8. Conclusions

The stress-strain behaviour of a climbing rope for heavy falls like the UIAA test fall can be explained by a relatively simple nonlinear viscoelastic model.
Specifically, our conclusions are the following:

1. The usual viscoelastic models like the SLS model where friction starts with the beginning of the fall cannot accurately describe the rope tension vs. time.

2. Because of the high fall velocity, adiabatic conditions prevail with a time-delay of the internal friction in the rope. The friction comes only into play after the force maximum has been reached. After that maximum, there is a fast force drop, almost without change of length where the stored energy is dissipated. Therefore the behaviour of a climbing rope during a fall is thermodynamically reminiscent of an Otto process.

3. The time-delay of the friction implies that at first only conservative forces are acting. This allows the determination of the force constants by regression methods. It turns out that a strong nonlinear force proportional to the elongation cubed is present.

4. Both time-delayed friction and the nonlinear force term lead to a Duffing oscillator which describes the measured forces-time curves very well. It can also explain an experiment measuring $F_{max}$ with varying fall masses and fall factors, where the linear model fails.

5. The precise measurements show fast oscillations of the second longitudinal mode coming from the rope mass. Its frequency for small elongations and its increased frequency near the maximum elongation as a nonlinear effect allows an independent determination of the force constants.

The achieved understanding of the rope properties is also a necessary condition for a better understanding of the important rope fracture process of successively executed falls discussed in a future paper.

## Acknowledgements

The author would like to thank the IFT University Stuttgart for providing the experimental data for several climbing ropes. Thanks also to Ira Leuthäusser for helpful discussions and critical reading of the manuscript.

  

**Appendix: Exact solution of the SLS model at its critical point**

Because there is no overshooting in the measured F(t) (Fig.2.2), realistic rope parameters are near the critical damping point without oscillations. The SLS model is now solved at this point.

We start with the Laplace transform of the SLS equation of motion (3.4)

$$y(s) = m\left(v_0 + \frac{g}{s}\right)\frac{cs + k_2}{mcs^3 + mk_2s^2 + +c(k_1 + k_2)s + k_1k_2} \qquad (A.1)$$

To solve this equation one has to calculate the roots of the cubic equation of the denominator which is in principle possible. At the critical point the solution is much easier, because only real and equal roots γ of the denominator exist[11]. It corresponds to the critical point of a Kelvin model (or damped HO) where the oscillatory solutions have been just disappeared and where damping provides the quickest approach to zero.

γ satisfies the following equation

$$mcs^3 + mk_2s^2 + +c(k_1 + k_2)s + k_1k_2 = mc(s + \gamma)^3 \qquad (A.2)$$

with the solution:

$$\gamma = \frac{9}{8}\frac{c}{m} = \sqrt{\frac{k_1 + k_2}{3m}} = \frac{1}{\sqrt{3}}\omega \quad \text{and} \quad k_1 = \frac{1}{8}k_2$$

Here the angular frequency $\omega = \sqrt{(k_1 + k_2)/m}$ was introduced. Because of the small $k_1$, the critical SLS model is close to the critical Maxwell model.
For g = 0 (a lengthy solution is also possible for g >0) one gets

$$y(s) = v_0\frac{s + 3\gamma}{(s + \gamma)^3}.$$

which leads after inverse Laplace transformation to

$$\begin{aligned} y(t) &= v_0t(1 + \gamma t)\exp(-\gamma t) \\ y_1(t) &= \frac{3}{2}v_0\gamma t^2\exp(-\gamma t) \\ \ddot{y}(t) &= -3v_0\gamma^2t\left(1 - \frac{1}{3}\gamma t\right)\exp(-\gamma t) \end{aligned} \qquad (A.3)$$

with the maximum values of $\ddot{y}$ and y

$$\ddot{y}(t_1) = \ddot{y}_{max} = a_{max} = -v_0\gamma\left(\sqrt{13} - 2\right)\exp\left(-\frac{1}{2}\left(5 - \sqrt{13}\right)\right) \qquad (A.4a)$$

$$y(t_2) = y_{max} = \frac{v_0}{\gamma}\left(2 + \sqrt{5}\right)\exp\left(-\frac{1}{2}\left(1 + \sqrt{5}\right)\right) \qquad (A.4b)$$

occuring at times

$$t_1 = \frac{1}{\gamma}\frac{1}{2}\left(5 - \sqrt{13}\right) = \frac{1}{\gamma}0.697 \text{ and } t_2 = \frac{1}{\gamma}\frac{1}{2}\left(1 + \sqrt{5}\right) = \frac{1}{\gamma}1.618$$

Eliminating γ from (4.4b) and inserting it in (4.4a) one gets $F_{max} = 0.672 \frac{mv_0^2}{y_{max}}$. Very surprisingly, it turns out that the relation is also exactly valid for g>0. The absorbed energy until $t_1$ is given by

$$\frac{E_A(t_1)}{E_0} = \left(1 - \left(208 + 57\sqrt{13}\right) \cdot e^{-(5-\sqrt{13})}\right) = 0.384 \qquad (A.5)$$

independent of γ. In this aperiodic case about one third of the initial energy until force maximum is dissipated.

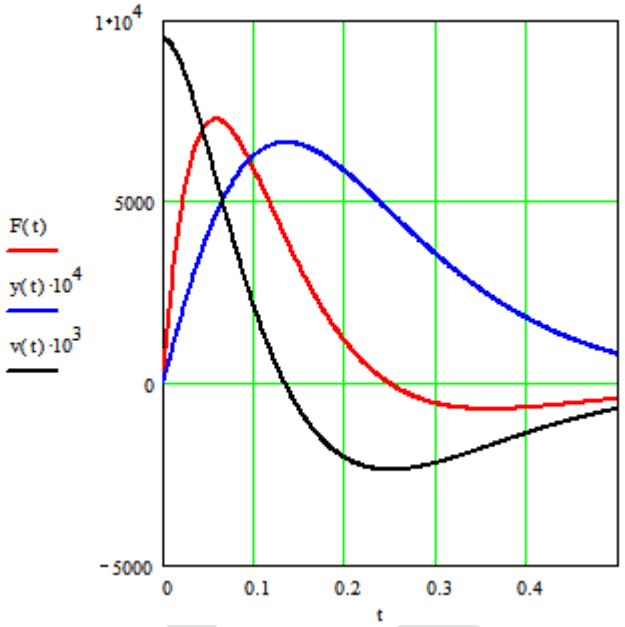


**Fig.A.1.** F(t), v(t) and y(t) for the critical SLS model for γ=12. A satisfactory fit with the measured F, v and y (see Fig.2.2) is not possible.

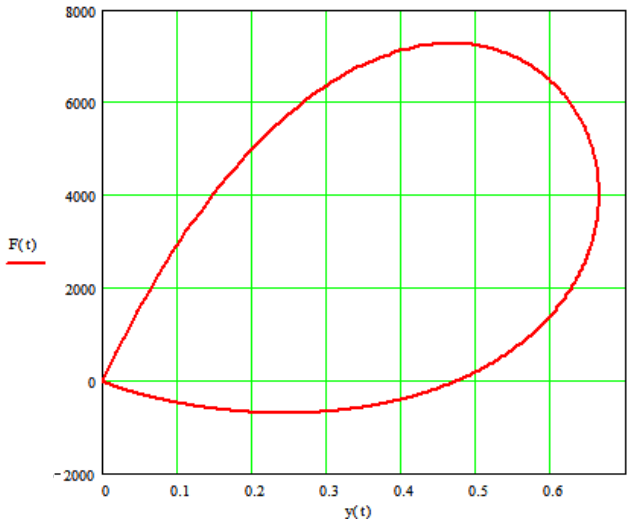


**Fig. A.2.** Typical round shaped hysteresis of the SLS model using γ=12.

The critical SLS model can also be used to describe time-delayed friction when calculated with the changed initial conditions (6.2).
Te solution for $t>t_1$ is given by

$$y(t) = \left[\left(y(t_1) - \frac{3g}{\gamma^2}\right)\left(1 + \gamma(t-t_1) - \gamma^2(t-t_1)^2\right) - 4gt^2\right]e^{-\gamma(t-t_1)} + \frac{3g}{\gamma^2} \qquad (A.6)$$

Although the physics of this model differs from the Kelvin model, it can also approximately explain F(t) and y(t) for $t > t_1$. Its energy absorption rate $\dot{E}_a$, however, is much more abrupt and faster than that of the Kelvin model (Fig.A.3).

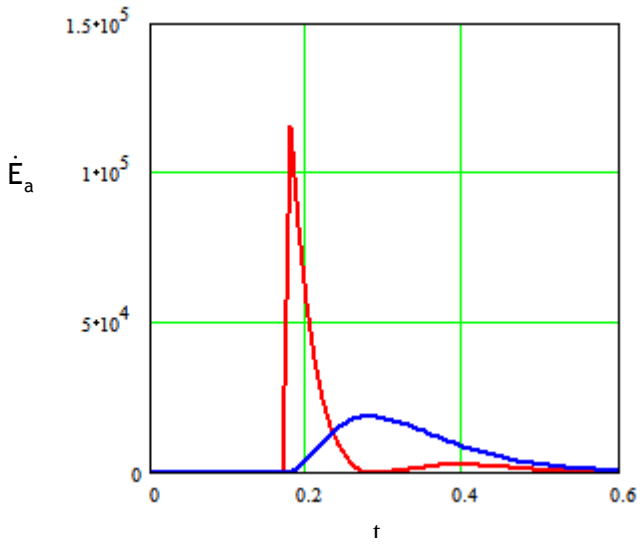


**Fig.A.3.** The energy absorption rate of the critical SLS model (red) compared with the Kelvin model (blue) both with delayed friction.

Unfortunately it is not possible to calculate $\dot{E}_a$ from the measured F alone, because it depends on the underlying model. The $\dot{E}_a$ for the SLS model is determined by its internal velocity $\dot{y}_i$. Expressing $\dot{y}_i$ only by observables, the energy absorption rate is given by $c\left(\dot{y} - \dot{F}/k_2\right)^2$ different from that of the Kelvin model. In contrast to the Kelvin model, the critical SLS model is very soft and its static elongation $\frac{3g}{\gamma^2}$ cannot explain the experimental elongation.

[1] http://www.theuiaa.org/safety-standards.html
[2] UIAA norm fall tests for climbing ropes , IFT, University of Stuttgart (2012)
[3] H.T.Banks, G.A.Pinter, “Damping: Hysteretic Damping and Models”, Encyclopedia of Vibration 01/2000 (2000)
[4] C.W.Bert, “Material damping: an introductory review of mathematical models, …“, Journal of Sound and Vibration 29(2), 129 (1973)
[5] M. Pavier, Experimental and theoretical simulations of climbing falls, Sports Engineering **1**, 79-91 (1998)
[6] A.Wexler, “The theory of belaying”, reprinted from THE AMERICAN ALPINE JOURNAL Vol.VII, 4 (1950)
[7] A.L.Wasserman, “Thermal physics”, Cambridge University Press (2012)
[8] R.Kubo, “Statistical mechanics“, North-Holland (1965)
[9] D.Arovas, “Lecture notes on thermodynamics and statistical mechanics”, CreateSpace Independent Publishing Platform
[10] C.Weber, "What heavy climbers need to know", http://www.safeclimbing.org/education.htm
[11] Y.M. de Haan, G.M.Sluimer, “Standard linear solid model for dynamic and time dependent behaviour of building materials”, HERON, Vol.46,1 (2001)